Final Report for NASA Contract 9-4411

Glenn M. Frye, Jr.

Principal Investigator

Physics Department

Case Western Reserve University

Cleveland, Ohio

R.G. Richmond, Technical Monitor

NASA Manned Spacecraft Center

Houston, Texas

Submitted May 20, 1970

Summary

Under Contract NAS 9-4411 the cosmic ray group at Case Western Reserve University has:

(1) Completed the design and construction of a large area, thin plate spark chamber for the detection of cosmic gamma radiation;

(2) Calibrated the spark chamber at the Cornell 2 GeV Electron Synchrotron;

(3) Measured the atmospheric gamma ray intensity as a function of altitude and geomagnetic latitude;

(4) Invesitgated the neutron and residual mass background which would be important on a satellite experiment, and

(5) Surveyed the northern hemisphere for sources of cosmic gamma rays.

A description of the results is included in the following final report for this contract.

ABSTRACT

In a search for cosmic gamma radiation above 50 MeV 60% of the northern hemisphere has been surveyed on four balloon flights at 2.5 mbar. Gamma rays were detected by the electron-positron pairs produced in the plates of a 30 gap spark chamber which is sensitive from 50 MeV to 2 GeV, has an angular resolution of 2.6° and an HWHM acceptance angle of 20°. Non-scattering single tracks are shown to be unresolved pairs. No point sources of γ rays were seen in the regions $270^{\circ} < \alpha < 135^{\circ}$, $7^{\circ} < \delta < 57^{\circ}$; $125^{\circ} < \alpha < 220^{\circ}$, $-12^{\circ} < \delta < 37^{\circ}$. Upper limits to a number of possible point sources such as the Crab Nebula, Cygnus A, Cyg XR-1, M 87, 3C 48, 3C 273, CP 1133, CP 1919, and the sun, were set in the ranges $E_{\gamma} > 50$ MeV, $(1\text{-}4)\cdot 10^{-5}$ γ's $cm^{-2}sec^{-1}$; $E_{\gamma} > 150$ MeV, $(1\text{-}2)\cdot 10^{-5}$ γ's $cm^{-2}sec^{-1}$; and $E_{\gamma} > 500$ MeV, $(0.5\text{-}1.5)\cdot 10^{-5}$ γ's $cm^{-2}sec^{-1}$. For the Crab these results imply an average magnetic field of $> 4\cdot 10^{-5}$ g and no direct production of synchrotron electrons from high energy p-p collisions. The limit for M 87 is an order of magnitude below Felten's curve which fits from 10^{8} to 10^{19} Hz. The main energy source for 3C 273 cannot be matter-antimatter annihilation. The flux from the galactic plane $-3^{\circ} < b^{II} < 3^{\circ}$, $55^{\circ} < \ell^{II} < 85^{\circ}$ exceeds neighboring areas in the ratio 1.2 ± 0.1 confirming the OSO-3 result, although no excess is seen in the direction of the galactic anticenter in disagreement with the satellite observation. The atmospheric γ ray flux at 2.5 mbar above 50 MeV at Palestine, Texas, vertical cutoff 4.6 GV, is $(2.9\pm0.6)\cdot 10^{-3}$ γ's $cm^{-2}sec^{-1}sr^{-1}$, and at Panama City, 11.9 GV, $(1.3\pm0.3)\cdot 10^{-5}$ γ's

$cm^{-2} sec^{-1} sr^{-1}$. Extrapolated to the top of the atmosphere the upper limit to the isotropic cosmic γ ray flux is $0.5 \cdot 10^{-3}$ γ's $cm^{-2} sec^{-1} sr^{-1}$.

$cm^{-2} sec^{-1} sr^{-1}$. Extrapolated to the top of the atmosphere the upper limit to the isotropic cosmic γ ray flux is $0.5 \cdot 10^{-3}$ γ's $cm^{-2} sec^{-1} sr^{-1}$.

1. INTRODUCTION

Recent discoveries in the x-ray and nuclear gamma ray portions of the spectrum have extended the upper limit of the observed electromagnetic spectrum to 10^{20} Hz. Over a decade ago, Morrison (1958) pointed out that, since high energy electrons must be present in strong radio sources to account for the radio-frequency synchrotron radiation, gamma rays with an energy above 50 MeV ($\sim 10^{22}$ Hz) might be produced in some astronomical objects with fluxes great enough to be detectable at the earth. Extensive calculations by several groups (Hayakawa, Okuda, Tanaka, and Yamamoto 1964; Gould and Burbidge 1967; Garmire and Kraushaar 1965; Ginzburg and Syrovatskii 1965; Fazio 1967) have shown that the most probable mechanisms for producing gamma rays of this energy are (1) the decay of neutral pions, (2) bremsstrahlung, and (3) inverse Compton scattering. Some of the possible candidates for point sources are the Crab Nebula, M 87, Cygnus A, 3C 273 and other QSO's, the sun, Scorpio XR-1, and the other strong x-ray sources. Evidence that the galactic plane is an extended source of high energy gamma rays has recently been found on an OSO-3 experiment by Clark, Garmire and Kraushaar (1968).

A number of groups have searched for point sources of cosmic gamma radiation with a variety of experimental techniques (Frye and Wang 1968); Fichtel, Cline, Ehrmann, Kniffen, and Ross 1968; Delvaille, Albats, Greisen, and Ögelman 1968; Duthie 1968; Fazio, Helmken, Cavrak, and Hearn 1968; Fegan, McBreen, O'Mongain, Porter, and Slevin 1968; Fazio,

Helmken, Rieke, and Weekes 1968; Anand, Daniel, and Stephens 1968). In this paper we report the results of four high altitude balloon flights in the northern hemisphere with a spark chamber system which has the largest area-solid angle factor of any detector yet used. Good exposures to the above named possibilities were obtained and, in particular, one flight was made from Panama where both M 87 and 3C 273 pass within 6° of the zenith. On none of these flights was any positive gamma ray signal ascribable to a point source detected above the diffuse atmospheric background, which is generated in the 2.5 g cm^{-2} of air above the balloon by the interaction of the primary cosmic radiation with atmospheric nuclei. The implications of these upper limits on cosmic gamma radiation will be discussed for various astrophysical models which have been proposed.

2. EXPERIMENTAL METHOD

The spark chamber employed for these flights (Fig. 1) is an enlarged version of the one described previously (Frye, Smith, Hruschka, Goff, and Zych 1966). The incident gamma ray is converted in one of the chamber plates into an electron-positron pair which then passes through the coincidence counter telescope. The anti-coincidence umbrella prevents charged cosmic rays from triggering the system. The logic circuitry accepts the $\bar{1}234$ combination of pulses and actuates the high voltage pulser so that an 8 kv pulse appears across each pair of chamber plates within 200nsec after the passage of the charged particles through the chamber. The resulting spark pattern shows the point of creation of the electron-positron pair in the chamber; the direction of the pair, which is closely related to the direction of the incident gamma ray; and gives a measure of the gamma ray energy from the multiple scattering of the electron and positron in the remaining chamber plates. The unique signature provided by two tracks originating at the same point in the chamber with an opening angle of, at most, a few degrees and the scattering typical of an electron serves to eliminate most of the other neutral cosmic radiation which can penetrate the anticoincidence screen and interact in the chamber. The two 90° steroscopic views of the chamber are recorded on a single frame of 16 mm Kodak Pan Dacomatic film. The photographic method of recording the spark pattern was chosen over the sonic or wire chamber methods in order to maximize the resolution in spark width and position and to

minimize the ambiguities in spark pattern recognition.

The experimental procedure is to fly the system so that the chamber axis is vertical, monitor the location of the balloon continuously during the flight, and record the instantaneous orientation of the chamber by magnetometers for each event. Then, from the direction of the pair in the chamber, the right ascension α and declination δ of each gamma ray is calculated.

The efficiency of the system for detecting gamma rays is a function of the angle θ between the γ-ray direction and the axis of the spark chamber normal to the spark chamber plates. This geometrical factor can be calculated numerically. In the actual data reduction, the first two gaps of the spark chamber were used to check the anticoincidence electronics. Therefore, an event was taken as a pair only if it originated in the third plate or below. Also, at least four gaps were required to define an event as a pair, so the production plates were #3 through #27. The variation as a function of θ is shown in Fig. 2 where the ordinate is the total effective spark chamber plate area A_e. Since the plates are square, there is also a slight azimuthal variation over which an average has been taken. During the flight a given point in the sky (α,δ) will sweep across the acceptance cone of the chamber and the total exposure will be governed by $(At) = \int A_e \, dt$. In general, the wide acceptance angle of the system allows a four hour exposure to a given point that does not pass too far from the zenith, although the effective exposure can be increased by decreasing the distance between

counters 2 and 3 + 4 and thereby enlarging the acceptance cone.

The launch site, launch time, time at altitude, residual atmosphere, and other relevant flight data are collected in Table 1.

3. DATA ANALYSIS

a) Classification of Events

The events in the chamber can be grouped into four categories:

1) Electron-positron pairs: 21%

2) Single tracks: 29%

3) Stars or multiple tracks: 11%

4) Spurious sparking --- no well-defined track visible. 39%

The last two categories were sensitive to the threshold settings of the counters, especially that of the Cerenkov counter. The gain on each counter was set so that a single minimum ionizing particle would be detected over the entire area of the counter. As a result the directional Cerenkov counter had an up-down ratio of only 3:1 for sea level mesons, indicating that either the blackened upper surface was still partially reflecting or that some scintillation light was also being detected. The thresholds were set this low to insure that the system still had a high efficiency for pairs in which the division of energy between the two particles was so asymmetrical that only one was sufficiently energetic to penetrate the entire counter telescope. Indeed, many events are seen in the chamber where one prong of the pair stops in the chamber itself. An alternative

TABLE 1

BALLOON FLIGHT DATA

Flight No.	Launch Site	Flight Duration At Altitude	Average Altitude
232-P	Palestine, Texas	0435-0845 UT, 7/19/66	2.32 mbar
234-P	Palestine, Texas	1351-1917 UT, 7/26/66	2.46 mbar
236-P	Palestine, Texas	0813-1228 UT, 7/31/66	2.89 mbar
1181-R	Panama City	1333-2032 UT, 9/22/66	2.92 mbar

procedure would have been to set the counter threshold so that a twice minimum pulse was required. Tests at sea level showed that the ratio of pairs to total events would have been higher, but the number of photons detected per unit time would have been less.

b) Identification of Events

The basic design criterion for the spark chamber system was for it to be a survey instrument and therefore to have as wide an acceptance angle and as large a gamma ray conversion efficiency as possible. Since the 30 spark chamber plates comprise almost a radiation length of iron, multiple Coulomb scattering and energy losses in the plates produce a variation in detection efficiency with position in the chamber. A low energy pair is more likely to have one of its prongs traverse the counter telescope if it is converted near the bottom of the chamber, because there the probability is greatest that it will not scatter out of the acceptance cone or lose too much energy in traversing the material between the point of conversion and the triggering counters. On the other hand, a high energy pair has a greater detection probability if it is converted near the top of the chamber, because there is a maximum of scattering material it must traverse before reaching the bottom and therefore a greater probability that the two prongs will separate enough so that the event will be recognizable as two separate tracks. The multiple sparking efficiency is also an important factor in recognizing an event as a pair. It is necessary to evaluate the efficiency of the chamber as a function of position and gamma ray energy in order to determine the atmospheric

flux and the upper limits to the flux from possible extra-terrestial sources. The variation in efficiency with position is also useful in identifying the single tracks.

An indication of the energy of each pair was made by measuring the separation of the two prongs of the pair. Since this separation is predominantly due to the multiple scattering of the electron and positron in the chamber plates, an energy, E_o, can be calculated if equipartition is assumed, i.e. that the γ-ray energy, E_γ, is divided equally between the electron and positron. If the energy division between electron and positron is asymmetric, then $E_\gamma > E_o$, and a more accurate γ-ray spectrum can be obtained by folding the known pair production differential cross section into the E_o spectrum. The resulting spectrum is too uncertain to quote as an actual measurement of the gamma ray spectrum (although the power law exponent at 1 GeV of - 1.8 agrees reasonably well with earlier determinations (Svennson 1958); Frye, Reines, and Armstrong, 1966) but it is sufficient for evaluating the results of the search for sources. We are in the process of determining E_γ more accurately by measuring the multiple scattering of each prong of the pair. These results will be presented at a later date.

The procedure adopted to determine the variation in efficiency with position in the chamber was to use the pairs observed during flight. If each section of the chamber had the same efficiency, the same number of events of a given energy would be observed in each section of the chamber except for the small corrections required

for variation in area-solid angle factor, and absorption and scattering by the material above. The observed variation in efficiency with position in the chamber is shown in Table 2 where the maximum number of events is aribtrarily taken as 100%. That this is a reasonable assumption is shown by calculations of event loss from multiple scattering and ionization energy loss and is borne out by the constant response over several sections of the chamber for the medium energy range. Averaging these curves over gaps 3-26 yields the values listed in the last column of Table 2. Only a small difference was seen between the Texas and Panama flights (see 3 d), so Table 1 is an average over the four.

Obviously, some very low energy and some very high energy pairs will be observed, depending on their point of origin in the chamber and the energy partition between the two prongs. The effective energy range of the system is set on the low energy side at E_γ = 50 MeV by requiring that any pair which originates in the lower third of the chamber (below gap 19) has enough energy to trigger the counter telescope. The effective upper energy limit of 2 GeV is set by requiring that a pair originating in the upper third of the chamber (above gap 40) separate on the average by 2 mm upon reaching gap 30.

Several mechanisms are possible for the production of the single tracks observed:

1) Unresolved pair

TABLE 2

SPARK CHAMBER EFFICIENCY

E_o(MeV)	Gap No. 3-6	7-10	11-14	15-18	19-22	23-26	Av. Eff.
0-40	0.35±0.06	0.44±0.07	0.65±0.09	0.92±0.13	1.00	0.30±0.06	0.61±0.06
40-70	0.67±0.09	0.58±0.08	0.83±0.10	1.00	0.69±0.09	0.17±0.04	0.66±0.05
70-100	0.82±0.11	0.97±0.12	0.98±0.12	1.00	0.47±0.07	0.08±0.03	0.72±0.06
100-150	0.77±0.08	0.82±0.09	1.00	0.84±0.09	0.21±0.04	0.02±0.01	0.61±0.05
150-200	0.89±0.10	1.00	0.64±0.08	0.43±0.06	0.23±0.04	0.01±0.01	0.52±0.05
200-300	1.00	0.89±0.10	0.66±0.08	0.43±0.06	0.13±0.03	0.01±0.01	0.52±0.04
300-500	1.00	0.79±0.09	0.65±0.08	0.18±0.03	0.03±0.01	0	0.44±0.04
500-1000	1.00	0.62±0.09	0.36±0.07	0.14±0.04	0.03±0.02	0.01±0.01	0.36±0.04
> 1000	1.00	0.78±0.25	0.17±0.10	0.22±0.11	0	0	0.36±0.09

2) Compton recoil

3) Photoproduction of a single pion

4) Neutron induced reaction with only one charged secondary

5) Charged particle albedo

The experimental information which is available for identification of the single tracks includes the γ-ray spectrum at altitude, the variation of production rate with position in the chamber, ascent data, zenith angle distribution, and multiple scattering in the chamber. For each single track, the scattering angle was measured as the difference between the initial and final directions of the track.

Possibility 3) can be eliminated at once since the photoproduction cross section and the measured γ-ray spectrum give a rate too small by a factor of 10^{-3} to account for the observed number of single tracks. Also, only the lowest energy single tracks can be Compton recoils, since the Compton cross section decreases with energy while the pair cross section increases. For iron they are equal at 10 MeV and have a ratio of 18 at 100 MeV.

The most significant information for the identification of the single tracks is the variation in production rate with energy and chamber position. In contrast to the pairs with E_o > 100 MeV, where the rate either remained constant or decreased with chamber depth, the number of singles at each energy with zenith angle < 30^o increased with chamber depth. This can only be explained by mechanism 1) or possibly 4). The number of unresolved pairs to be expected can be

predicted by applying multiple scattering theory to the number of pairs observed for each energy and chamber position. The total number of pairs, N_T, is given by

$$N_T = N_o \exp[a^2/s^2]$$

where N_o is the number observed, s is the prong separation and is a function of energy and chamber position, and a is related to the minimum separation which can be observed. It is found that the data for the upper half of the chamber, $200 < E_o < 1000$ MeV, can be fitted by a = 0.41 cm. The total number of unresolved pairs on the four flights is then calculated to be 3202. The number of single tracks observed, $E_o > 100$ MeV is 3407. Therefore, in the directional analysis (see 4 c) both the pairs and singles with $E_o > 100$ MeV will be considered as γ-ray events.

The rest of the single tracks with $E_o < 100$ MeV show significant scattering and, if they are downward moving particles, must be either electrons or muons. There is also the possibility that there is a contribution from charged particle albedo 5) since the up-down ratio of the Cerenkov counter was low. However, the albedo could at most be a small fraction of the total since the stopping albedo tracks would be distributed approximately equally throughout the chamber.

c) Event Rate vs. Altitude

On each flight the apparatus was turned on during ascent at an altitude where the residual atmospheric pressure was about twice that at the float altitude. The average ascent rate was too rapid

(∿ 200 m/min.) and the dead time of the system too long (190 msec) to achieve a statistical accuracy during ascent that was commensurate with that at ceiling. However, the variation in count rate with altitude is useful in identifying the nature and source of the various types of events. Secondaries produced in the atmosphere at these altitudes will have an intensity proportional to residual atmosphere, whereas any effect due to the interaction of the primary radiation with the gondola itself will be independent of atmospheric depth since the atmospheric depth is small compared to the nuclear interaction length of 140 gm cm^{-2}. During each flight the pressure was recorded at two minute intervals by a Wallace and Tiernan Type FA160150 gauge which had a known temperature coefficient. It was calibrated before each flight and had an accuracy of 0.1 mbar.

Each of the four classes of events of Sec. 3a with a zenith angle < 30° showed a rate proportional to the residual atmosphere which extrapolated to a zero rate at the top of the atmosphere. In particular, as is shown in Fig. 3, the single tracks exhibit the same linear behavior with atmospheric depth as the resolved pairs. Therefore the variation with altitude of the single tracks is consistent with their identification as unresolved pairs.

d) Geomagnetic Variation

The vertical geomagnetic cutoff at Palestine is 4.6 GV and at Panama City is 11.9 GV (Quenby and Wenk 1958). Therefore a harder γ-ray spectrum would be expected at the latter site. Our results

show some evidence for such an enhancement of the high energy part of the spectrum. For Texas and Panama the ratios of the number of pairs in the E_o energy intervals 0-100, 100-500, and > 500 MeV are (1.00):(1.32±0.05):(0.16±0.01) and (1.00):(1.45±0.10):(0.24±0.03) respectively where only the statistical uncertainty is indicated.

The flux of primary cosmic ray decreases by a factor 3 from the 600 protons $m^{-2}sec^{-1}sr^{-1}$ observed in Texas (Daniel and Sreenivasan 1965, Oran, Frye, and Wang 1969). The flux of atmospheric γ-rays should decrease by a somewhat lesser factor since the pion multiplicity increases with energy in proton-nucleon collisions. The ratio of the number of pairs per unit time at 2.5 mbar in Texas to the number in Panama is 2.26 ± 0.28. The same ratio of single tracks with energy > 150 MeV is 1.72 ± 0.26. The ratio is 2 for each within the statistical accuracy and a lower value for the single tracks is anticipated, since, if they are unresolved pairs, they represent the higher end of the spectrum. Therefore the geomagnetic variation is also consistent with the interpretation of the single tracks as unresolved pairs.

e) Zenith Angle Distribution

If the γ-rays observed are atmospheric secondaries, the angular distribution as a function of the zenith angle should increase as sec θ. The area-efficiency factor of the spark chamber (Fig. 2) is accurate out to ~ 30° before the thickness of the Cerenkov detector

introduces an appreciable uncertainty. Fig. 4 shows that the number of pairs and single tracks divided by $A_e \sec\theta$ is flat to within the statistical accuracy over the range $0^\circ < \theta < 27^\circ$, i.e. consistent with atmospheric production.

f) Neutron Background

Since a neutron can penetrate the anticoincidence counters and interact in the chamber, the secondaries from the neutron star will simulate a pair if there are only two energetic prongs which do not have too large an included angle. The number of such events can be estimated by combining the nuclear emulsion data on the prong distribution in high energy interactions with the number of definite neutron events seen in the chamber which have three or more prongs. We find the ratio of all possible neutrons stars to electron positron-pairs is $\leq$ 50%. In nuclear emulsion exposed to 6 GeV protons < 2% of the events have two prongs of energy > 40 MeV and an included angle $\leq 30^\circ$ (A. D. Zych, private communication). Therefore if one assumes the prong distribution is the same for cosmic ray neutrons in iron as it is for 6 GeV protons in emulsion, neutrons contribute $\lesssim$ 1% of the observed pairs. A similar conclusion is obtained using the Bristol result (Camerini, Davies, Fowler, Franzinetti, Muirhead, Lock, Perkins, and Yekutieli 1952) that $\sim$ 4% of the cosmic ray neutrons stars observed in emulsion have two and only two high energy prongs.

Since the number of neutron events in the chamber is a significant fraction of the number of pairs, it is obvious that the detection system must be able to distinguish between the two types of events with high

efficiency. The neutron secondaries are still relativistic enough to trigger the Cerenkov counter in the counter telescope and only the visual properties of the spark chamber allow one to separate multi-prong events from pairs.

g) Residual Mass Background

Another potential source of background is the generation of γ-rays in the gondola itself by the charged primary cosmic radiation. The anticoincidence scintillators eliminate most of this effect but there is always the possibility of evading these guard counters. The most probable mechanism of this type is for the charged primary to interact with the outer covering of the anti-counter or with the scintillator itself in such a way that no charged secondaries are produced; or if there are charged secondaries, they escape without giving a detectable pulse from the anticounter. Since the present limits on the γ-ray flux are $\sim$ 1% of the charged particle flux, it is still possible for rare interaction modes to have an appreciable effect. This type of consideration will be even more important for future experiments with increased sensitivity, particularly those on satellites, where great effort is expected to escape the last 1/4% of the atmosphere. This effort will be negated if an "equivalent atmospheric effect" is produced by the residual mass above the chamber.

The design of our pressure seal for the spark chamber was such that most of the mass of the lid was above the top anticoincidence

counter. This was done to minimize the mass below the anticoincidence counter but above the sensitive volume of the chamber. The average thickness of the magnesium lid was 0.4 cm, except directly over the chamber walls (Fig. 1) where there was a ridge 2.5 cm wide and 2 cm thick. To see if this ridge was acting as a γ-ray source, the intersection of each observed γ-ray direction with the plane of the lid was calculated. No peak was seen at the position of the ridge, and therefore one gram of Mg placed directly above the anticoincidence counter and exposed to the primary charged particle cosmic radiation simulates a source of $< 1.10^{-7} \gamma$'s $cm^{-2} sec^{-1} sr^{-1}$. In the flights reported here this amounts to an effect of < 1%.

h) Angular Resolution

The angular resolution of the detector system is one of the most important factors in determining the threshold sensitivity for the detection of a point source of γ-rays in the presence of the atmospheric background. The threshold varies inversely with the angular resolution Ω , where Ω is defined as the half angle of the cone which includes half of the events. The predominant mechnaism for producing the finite angular resolution is the multiple scattering of the electron and positron in the four chamber plates over which the direction is measured. The ultimate limit on the angular resolution for any γ-ray detection in this energy range is set by the intrinsic opening angle of the pair. For example, at E_γ = 100 MeV the intrinsic opening angle of a pair is 1.4° (Olsen 1963) whereas that produced by multiple scattering, assuming equipartition, is 5.2°. Both vary inversely

with the energy of the γ ray.

We have measured the angular resolution of our chamber by exposures to the Cornell synchrotron at E_γ = 0.28, 0.72, and 1.21 Gev. The results can be fit by $\Omega_o = [(0.40/E_\gamma)^2 + 0.56^2]^{1/2}$ degrees where the second term is independent of energy and includes effects due to spark width, spark jitter, non-linearity in the optical system, etc. Also exposures at $\theta = 0^\circ$, 10°, 20°, and 30° show that $\Omega_o \propto (\sec\theta)^{5/2}$ as expected from multiple scattering. When averaged over the observed γ-ray spectrum and over θ, $\langle\Omega^2\rangle^{\frac{1}{2}} = 2.5^\circ$, $E_\gamma > 50$ MeV. Finally, Ω_o must be combined with the 0.5° angular uncertainty in the magnetometer determination to give a final $\langle\Omega^2\rangle^{\frac{1}{2}} = 2.6^\circ$, $E_\gamma > 50$ MeV.; 1.3°, $E_\gamma > 150$ MeV.; and 1.0°, $E_\gamma > 500$ MeV.

4. EXPERIMENTAL RESULTS

a) Atmospheric Flux

The average of the three Texas flights yields a value for the vertical atmospheric flux at 2.5 mbar of γ-rays above 50 MeV of $(2.9 \pm 0.6)10^{-3}$ γ's $cm^{-2}sec^{-1}sr^{-1}$. This result has been corrected for the dead time of the system and for absorption in the chamber and the anti-coincidence counter. The pair production cross section was averaged over the observed γ-ray spectrum. The linear dependence of the atmospheric flux on atmospheric depth has been utilized to normalize each flight to 2.5 mb. Also the sec θ production variation has been averaged over the 30° half angle acceptance cone in arriving

at the vertical flux. The 20% uncertainty in the absolute flux results primarily from the uncertainties in the dead time, 10%; the absorption above the chamber, 5%; the variation in efficiency with chamber depth (See 3 b), 10%; and the multiple scattering correction to the area-solid angle factor, 10%.

Similarly, the flux observed in Panama, normalized to 2.5 mbar, is $(1.3 \pm 0.3)10^{-3}$ γ's $cm^{-2}sec^{-1}sr^{-1}$. The ratio of the two fluxes is 2.20 ± 0.22 and has a smaller uncertainty than either absolute flux since only the statistical factor and the variation in dead time and chamber efficiency contribute.

b) Upper Limit to the Isotropic γ-ray Flux

When the data for singles and pairs of Fig. 3, a and b are combined and expressed in flux units, the resulting least squares fit is $F(y) = (-0.14 \pm 0.33) + (1.20 \pm 0.13)y$ γ's $cm^{-2}sec^{-1}sr^{-1}$ where y is the atmospheric depth in mbar. For the Panama flight $F(y) = (-1.25 \pm 0.77) + (1.02 \pm 0.27)y$ γ's $cm^{-2}sec^{-1}sr^{-1}$.

Therefore the upper limit to the isotropic flux at the top of the atmosphere is, with 95% confidence, for $E_\gamma > 50$ MeV, $0.5 \cdot 10^{-3}$ γ's $cm^{-2}sec^{-1}sr^{-1}$. This result is not in conflict with the possible isotropic flux found on OSO-3 of $1.1 \cdot 10^{-4}$ γ's $cm^{-2}sec^{-1}sr^{-1}$ above 100 MeV (Clark et al. 1968).

c) Upper Limits on Point Sources

The statistical problem of searching for a point source of γ-rays in the presence of the atmospheric background is complicated by the varying exposure, $(At) = \int A_e dt$, to different portions of the celestial sphere. If each unit of solid angle had equal exposure, then the distribution of the number of atmospheric γ-rays per unit solid angle would be Poissonian. We have adopted the following procedure for this analysis: (1) The direction of each event is plotted on a grid of α vs sinδ. On this cylindrical projection equal areas have equal solid angles. (2) The plot is divided into strips of width .04 in sinδ. (3) The relative exposure $\int A_e dt$ was calculated in 3° steps in α and δ for the scanned portion of the sky. (4) The direction with the maximum exposure was taken as the center of a rectangle which was given a 3° width in right ascension. (5) Proceeding to left and right from this point a computer program calculated the width of adjoining rectangles so that the product of $\int A_e dt$ and the solid angle remained constant. In other words bin sizes were chosen in such a way that an increase in solid angle compensated for the decrease in exposure to a given direction. The bin sizes so generated should therefore contain the same number of atmospheric events except for statistical fluctuations. Plots of this type for pairs from the four flights are shown in Fig. 5a, b, c, and d. χ^2 tests showed the distribution to be Poissonian with probabilities of 0.40, 0.51, 0.11, and 0.47 respectively. Similar density plots for the single tracks with $E_o > 100$ MeV gave 0.17, 0.65, 0.81, 0.95. As a result we conclude the background does indeed follow a Poisson distribution

and the subsequent analysis will be based on this distribution.

First one may look to see if the density in any bin exceeds that to be expected from the tail of the Poisson distribution. Both the equal exposure bins of Fig. 5 and an alternate set of equal sized bins ($\Delta\alpha = 3^{\circ}$, $\Delta\sin\delta = .04$) were examined. Six bins out of the central 1114 of Fig 5 had a cumulative Poisson probability $\leq .0045$ where statistically one would expect five. Also the largest bin was 4.1 σ above the mean which is not a significant excess. Since the question is often asked as to what is the largest γ-ray point source which might have been seen, the six regions were examined in more detail and the 2.6° cone found which included the largest number of events (Table 3). It should be emphasized that there is no evidence for these high density areas being other than statistical fluctuations. The apparent flux for five of the directions is $(1\text{-}2)10^{-5}\gamma$'s $cm^{-2}sec^{-1}$. The apparent flux from $\alpha = 154^{\circ}$, $\delta = +34^{\circ}$ is higher because the events are clustered in one section of the equal exposure bin and this is in an oblique direction which received only 20% of the maximum exposure.

Second, one can look in given directions to set upper limits on the γ-ray flux from various objects which have been suggested as possible γ-ray sources. The usual procedure in setting the upper limit has been to observe the number of events N_o from the source direction which fall within the angular resolution circle. Then for a 95% confidence limit the mean, μ, is calculated for the Poisson distribution which has a 5% probability for giving N_o or less events.

TABLE 3

DIRECTIONS FROM WHICH THE GREATEST NUMBERS OF EVENTS WERE SEEN*

Position		No. of Events	Background No. of Events	Apparent Flux γ's $cm^{-2} sec^{-1}$
α	δ			
73°	$+25^\circ$	25	13.5	$2 \cdot 10^{-5}$
80°	$+18^\circ$	17	11.2	$1 \cdot 10^{-5}$
154°	$+34^\circ$	11	1.8	$9 \cdot 10^{-5}$
172°	$+10^\circ$	20	10.2	$2 \cdot 10^{-5}$
190°	$+10^\circ$	16	10.2	$1 \cdot 10^{-5}$
281°	$+34^\circ$	24	14.4	$2 \cdot 10^{-5}$

*See Sec. 4 c

However, $\mu = N_b + N_s$ where N_b is the number of events predicted for the atmospheric background and N_s is the number ascribable to the source as a 95% confidence upper limit. Then the limit to the flux may be found from

$$F = N_s[C_a\ C_m\ C_r\ C_d/(At)C_\gamma]\ \gamma\text{'s cm}^{-2}\text{sec}^{-1}$$

where $C_a = 1.05$ is the correction for atmospheric absorption; $C_m = 1.10$, the correction for material above the chamber; $C_r = 2$, the correction for events outside the resolution cone; $C_d = 1.19 -- 1.30$, correction for dead time; (At) is the effective area-time factor, (See Table 4); and $C_\gamma = 1.64 \cdot 10^{-2}$, the average conversion efficiency per spark chamber plate. Of course, if a statistically significant signal were observed above background, then N_s would be the number of events due to the source and F the actual flux.

Recently, Hearn (1968) has developed a modification of the above procedure for calculating N_s based on the maximum likelihood method which converges to the same result if $N_o >> N_B$, is about 10% larger for $N_o = N_B$, and approaches the constant value $N_s = 3$ when $N_o << N_B$. This approach avoids the unphysical possibility of $N_s < 0$ and will be adopted here since in each case it gives a more conservative upper limit.

In Table 4 are listed the 95% confidence upper limits to the γ-ray flux for three energy thresholds: $E_\gamma = 50$, 150, and 500 MeV. The limits improve as the energy threshold is increased primarily because of the reduced background and smaller angular resolution circle.

TABLE 3

UPPER LIMITS TO THE γ RAY FLUX FROM POSSIBLE SOURCES IN THE NORTHERN HEMISPHERE

							E_o > 50 MeV			E_o > 150 MeV		E_o > 500 MeV
Object	α	δ	(At) $cm^2 sec. 10^7$	No. of Bkgrnd. Events N_B	No. of Events Observed N_o	Upper Limit To Flux 95% Conf. I_{95} $10^{-5} cm^{-2} sec^{-1}$	N_B	N_o	F_{95} †	N_B	N_o	F_{95} †
ornell #1*	6.8°	48.5°	7.12	14.8	12	1.7	2.8	3	1.3	0.8	2	1.3
ndromeda Neb.	10.5	41	9.7	20.1	20	1.8	3.9	4	1.0	1.1	1	0.7
ornell #2*	22.5	28.5	7.59	15.8	28	5.1	3.0	3	1.1	0.8	0	0.7
C 47	23.4	20.7	6.39	13.3	16	3.0	2.6	2	1.2	0.7	0	0.8
C 48	23.7	32.9	8.75	17.8	23	3.0	3.5	7	1.8	1.0	1	0.8
TA 21	49.1	16.3	3.56	4.8	5	3.0	1.2	0	1.4	0.2	0	1.4
erseus A	49.1	41.4	5.80	9.7	11	2.6	1.9	1	1.1	0.5	0	0.9
TA 33	74.4	46.4	8.20	11.6	7	1.1	2.4	3	1.1	0.5	3	1.1
rab Neb.	82.9	22	10.22	14.4	16	1.7	3.0	3	0.9	0.6	0	0.5
WRU #1*	83.3	39.1	11.34	16.0	23	2.5	3.3	2	0.6	0.7	0	0.4
C 147	84.7	49.8	5.69	8.0	9	2.5	1.7	1	1.3	0.7	1	0.9
C 443	93.5	22.6	10.57	14.9	18	2.0	3.1	2	0.6	0.7	1	0.6
C 196	120.5	48.6	4.26	6.0	6	2.6	1.2	1	1.6	0.3	1	1.6
un	123.9	19.4	5.88	8.6	9	2.3	1.7	1	1.0	0.4	0	0.9
P 1133	173.2	16.1	9.64	9.7	12	1.9	2.0	4	1.4	0.6	1	0.8
un	179.1	0.3	8.86	8.9	12	2.3	1.8	4	1.5	0.6	2	1.2
C 273	186.6	2.3	9.13	9.2	11	1.8	1.9	5	1.7	0.6	2	1.2
87	186.6	21.8	9.98	10.0	10	1.5	2.1	5	1.5	0.6	2	1.0
C 286	202.2	30.8	4.18	4.2	6	3.4	0.9	2	2.4	0.3	1	1.9
C 287	202.1	25.4	6.31	6.3	3	1.3	1.3	2	1.5	0.4	0	0.9
C 380	277.1	48.7	4.57	7.7	7	2.5	1.5	2	1.9	0.4	1	1.6
P 1919	289.8	21.8	9.02	15.2	14	1.6	2.9	3	1.0	0.8	1	0.8
C 400	290.2	14.1	6.08	10.3	16	4.0	2.0	4	2.0	0.6	0	0.8
ygnus A	299.5	40.6	9.44	16.0	15	1.6	3.0	4	1.2	0.9	2	1.0
ygnus XR-1	299.1	35.1	10.80	18.2	24	2.5	3.5	4	1.0	1.0	0	0.5
ochester #1*	304	35	10.60	17.9	16	1.4	3.4	4	1.0	1.0	0	0.5
yg. X	306.8	27	10.10	17.1	18	1.8	3.2	5	1.3	0.9	1	0.7
B 21	311	50.3	4.37	7.4	5	2.1	1.4	1	1.5	0.4	0	1.3
P 2015	311.2	28.5	8.98	15.2	18	2.3	2.9	2	0.8	0.8	1	0.8
yg. Loop	312.5	30	9.21	15.6	10	1.1	3.0	2	0.8	0.8	1	0.8
yg. XR-2	325.7	38.2	4.95	8.4	9	2.8	1.6	1	1.3	0.5	1	1.3

* See Sec. 5 g

† Same units as column 7.

5. DISCUSSION--COMPARISON WITH ASTROPHYSICAL MODELS

a) Crab Nebula and Other Supernova Remnants

It is well known that the radiation from the Crab Nebula is synchrotron radiation extending to the visible, $\nu = 10^{15}$ Hz and very possibly up to the hard x-ray region, $\nu = 10^{20}$ Hz. Any model of the Crab Nebula must either have an inherent lifetime for relativistic electrons which is >> 900 yrs. or provide a continuous source of electrons with energies up to at least 10^{12} ev. Burbidge (1958) suggested that the electrons are secondaries which are continuously produced in high energy p-p collisions via the rapid π-μ-e decay. Savedoff (1959) pointed out that this hypothesis could be tested experimentally by searching for the high energy γ rays which are produced in the decay of the accompanying neutral pions. The p-p pion production process is such that to a very close approximation the γ ray-electron ratio is one. The problem of deducing the electron flux from the observed electromagnetic spectrum has been treated by several authors. Savedoff originally estimated a flux at the earth from the Crab of $7 \cdot 10^{-5}$ γ's $cm^{-2} sec^{-1}$ for $B = 10^{-2}$ g while Gould and Burbidge (1967) give $1.5 \cdot 10^{-5}$ γ's $cm^{-2} sec^{-1}$ for $E_\gamma > 50$ MeV and $B = 10^{-4}$ g and $0.5 \cdot 10^{-5}$ γ's $cm^{-2} sec^{-1}$ for $E_\gamma > 500$ MeV. These latter values are very close to the upper limits set in this experiment. Therefore, the production of secondary electrons via high energy p-p interactions is improbable. Cerenkov shower results at 10^{12} ev (Fazio, Helmken, Rieke and Weeks 1968b) have also reached

this conclusion since they have set limits one or two orders of magnitude below the predicted flux. However, it has been suggested that the secondary production process could still be operative if the electrons produced were of lower energy and later were accelerated to 10^{12} ev. This possibility is eliminated by our experiment since the energy region observed, $5 \cdot 10^{7}$ -- $2 \cdot 10^{9}$ ev, is just the energy band of most of the electrons produced in the p-p, π-μ-e process.

Gould (1965) has considered inverse Compton collisions between the synchrotron photons and the high energy electrons within the volume of the Crab. The only poorly determined parameter here is the magnetic field. Apparao (1967) has found a very similar result for inverse Compton scattering of the universal black body radiation. Since the spectral index of the resulting γ rays in the interval 10^{22} - 10^{26} Hz reproduces the spectral index of 0.3 found in the 10^{7} - 10^{14} Hz region which is much flatter than the index for the atmospheric background, the most sensitive comparison can be made at $E_\gamma > 500$ MeV ($\sim 10^{23}$ Hz). Our upper limit is $F_\gamma < 0.5 \cdot 10^{-5}$ γ's $cm^{-2} sec^{-1}$ which implies an average magnetic field over the volume of the Crab $> 4 \cdot 10^{-5}$ g.

It has been shown (Haymes, Ellis, Fishman, Kurfess, and Tucker 1968) that the single curve which fits the optical and soft x-ray spectrum with the spectral index of 1.2 extends to 0.5 MeV (10^{14} - 10^{20} Hz). Their count spectrum of $dN/dE = 7\ E^{-2.2}$ photons $cm^{-2} sec^{-1} keV^{-1}$ predicts a counting rate of $(1.5 \pm 1.0) \cdot 10^{-5}$ γ's $cm^{-2} sec^{-1}$ for $E_\gamma > 50$ MeV, which is not in disagreement with our upper limit of

$1.7 \cdot 10^{-5}$ γ's $cm^{-2} sec^{-1}$. It would not be surprising to see the spectral index increase above 10^{21} Hz, if synchrotron radiation is the dominant mechanism, since this implies a maximum electron energy $\sim 10^{15}$ eV for B = 10^{-4} g and a gyromagnetic radius $\sim 10^{-2}$ the radius of the Crab.

At $2 \cdot 10^{12}$ eV Fegan et al. (1968) obtained an indication of a positive flux of $1.5 \cdot 10^{-10}$ γ's $cm^{-2} sec^{-1}$ although this has not been confirmed (Fazio et al. 1968b). Such a flux would imply an almost flat energy spectrum between 10^{7} eV and 10^{12} eV.

In addition, the supernova remnants HB9, OA 184, VRO 42.05.01, Sh 147, Sh 34, IC 443, HB 21 and the Cygnus loop from the list of Poveda and Woltjer (1968) were included in this survey and those with the highest radio flux are included in Table 4.

b) M 87

The galaxy M 87 with its associated jet is one of the strongest radio sources and is the first extra-galactic x-ray source to be observed (Bryam, Chubb, and Friedman (1966). Shklovski (1967) pointed out that the same spectral index fits all the observations from the radio to the soft x-ray region. Felten (1968) has discussed various models for the jet and has shown that the entire spectrum from 10^{8} to 10^{18} Hz can be fitted by the equation $F_{\nu} = 1.38 \cdot 10^{-18} \nu^{-2/3}$ W m^{-2} Hz^{-1}. Recently Haymes, Ellis, Fishman, Glenn, and Kurfess (1968) have detected x-rays up to 100 keV which, in conjunction with the soft x-ray results of Bradt, Mayer, Naranan, Rappaport and Spada (1967),

can be fitted with the same spectral index. However, the flux observed by Bradt et al. (1967) is a factor of four less than predicted from Felten's spectrum. Moreover this equation predicts a flux of γ rays between 50 MeV and 5 GeV of $1 \cdot 10^{-4}$ γ's $cm^{-2} sec^{-1}$ i.e. an order of magnitude above the upper limit set by this experiment. Therefore, the spectral index gradually increases above 10^{23} Hz.

Felten has also considered the secondary production process to account for the presence of relativistic electrons throughout the jet. Above $E_\gamma = 5 \cdot 10^{11}$ eV the model predicts a flux an order of magnitude greater than the experimental upper limits (Chudakov et al. 1963; Fazio et al. 1968b). Either the magnetic field must have the low value $B = 10^{-5}$ g or the electrons must have been further accelerated after the original p-p production. Unfortunately, our experiment is not sensitive enough to detect the predicted flux for $E_\gamma > 50$ MeV. Felten (1968, eq. 19) predicts a flux of $\sim 10^{-7}$ γ's $cm^{-2} sec^{-1}$, two orders of magnitude below our sensitivity.

c) Other X-ray Sources

In addition to the Crab Nebula and Virgo A, the four x-ray sources in the Cygnus portion of the galactic plane were also included in the survey. A region including Cyg X-1 had earlier been identified as a possible γ-ray source (see g) below). The upper limits to the γ-ray flux are all $\simeq 10^{-5}$ γ's $cm^{-2} sec^{-1}$.

d) Quasi-Stellar Objects

The QSO's 3C 47, 48, 147, 196, 273, 286, 287, 345, and 380 have been analyzed specifically. 3C 273 has been treated in detail earlier (Frye and Wang, 1968) and the conclusion arrived at there, that the basic energy source for 3C 273 cannot be matter-antimatter annihilation, is not affected by the final data analysis presented here. It may be possible in the future to sharpen this conclusion further when an energy measurement is available for each γ ray, since the $p\bar{p}$ annihilation γ's are sharply peaked compared to the atmospheric background. For instance, the energy interval 50-200 MeV contains 50% of the annihilation events and only 25% of the atmospheric background spectrum.

The inverse Compton process is also expected to be of significance for QSO's since many have been shown to have very small angular widths implying a very high photon density. Ginzburg and Syrovat-Skii (1963) have calculated a flux of γ rays $\sim 10^{-5}$ γ's $cm^{-2}sec^{-1}$ from 3C 273. Such calculations are model dependent but the experimental upper limit found in this experiment does provide a constraint on the product of photon density and electron flux for any QSO model.

e) Pulsars

Recent observations of Cerenkov light from extensive air showers by O'Mongain, Porter, White, Fegan, Jennings, and Lawless (1968) and Charman, Jelley, Orman, Drever, and McBreen (1968) have given evidence for γ rays from CP 1133 of $5 \cdot 10^{-11}$ γ's $cm^{-2}sec^{-1}$ at $3 \cdot 10^{12}$ eV and

$2 \cdot 10^{-12}$ at $7 \cdot 10^{13}$ eV. Fazio et al. (1968c) have failed to confirm the lower energy result for pulsed emission at the pulsar frequency. If the positive result is established at $\sim 10^{13}$ eV, it would again imply a flat energy spectrum over the interval 10^{22} to 10^{27} Hz. CP 1919, NP 0532, NP 0527 and AP 2015 were also surveyed.

f) The Sun

Dolan and Fazio (1965) have calculated that neutral pion decay would be the most likely source for high energy gamma rays during a solar flare. Elliot (1964) has proposed a flare model in which γ radiation would be a precursor of the optical flare. During our two flights (232 and 1181) which viewed the sun only subflares occurred. If the data from the two flights are combined, the upper limit to the quiet sun γ-ray flux becomes $1.6 \cdot 10^{-5}$ γ's $cm^{-2} sec^{-1}$ for $E_\gamma > 50$ MeV.

g) Previously Reported Possibilities for Gamma Ray Point Sources

Earlier experiments with the "first generation" of spark chambers by Ögelman, Delvaille and Greisen (1966), Duthie, Cobb and Stewart (1966), and Frye and Smith (1966) each found directions from which the number of pairs was greater than the atmospheric background although only at the (2-3)σ level. If real, the indicated fluxes were $\sim 2 \cdot 10^{-4}$ γ's $cm^{-2} sec^{-1}$ and should have been detected here. These possibilities are labeled Cornell #1 and #2, Rochester #1, and CWRU #1 in Table 4. None indicates a number of events significantly

different from the background level. Cornell #2 does have 28 events compared to the expected background of 15.8 events. However, their threshold was 1 GeV and our limit for $E_\gamma > 500$ MeV is $0.7 \cdot 10^{-5}$ $cm^{-2} sec^{-1}$, an order of magnitude less than their apparent flux. Therefore, unless there have been unusual time variations, these effects were due to statistical fluctuations and the apparent excesses discussed in Sec. 4 probably arise from similar effects.

h) Diffuse Gamma-Ray Emission from the Galaxy

The high energy γ-ray flux to be expected from neutral pion decay, bremsstrahlung, and inverse Compton scattering has been calculated by several authors and summarized by Fazio (1967). Good evidence for such emission from the galactic plane with the peak signal coming from the center of the galaxy has been found with a counter experiment on OSO-3 by Clark et al. (1968). Their flux from the galactic center of 5×10^{-4} γ's $cm^{-2} sec^{-1} rad^{-1}$ for $E_\gamma > 100$ MeV is a factor ~ 25 greater than had been predicted.

We have analyzed our results for the two regions of the galactic plane - $3^\circ < b^{II} < 3^\circ$; $55^\circ < \ell^{II} < 85^\circ$ and $165^\circ < \ell^{II} < 195^\circ$ where we have the maximum exposure. Only events where $E_\gamma > 100$ MeV were taken to provide a direct comparison. We find 135 events from Cygnus in the region $|b^{II}| < 3^\circ$ compared to 301 in the neighboring strips $3^\circ < |b^{II}| < 12^\circ$. After a 10% correction for relative exposure, the ratio of flux from the galactic plane compared to adjacent areas is 1.23 ± 0.13 where the uncertainty is statistical only. In the

direction of the galactic anticenter the same ratio is 1.01±0.11.

Several tentative conclusions can be drawn from these data where it should be kept in mind however that the positive ratio seen by us in Cygnus is only 2σ. (1) The magnitude of the flux given by Clark et al. (1968) may be high by a factor two or three since their result predicts we should see a ratio of 1.6. (2) The effect is confined to the galactic plane to within our resolution of $\pm 3^{\circ}$. (3) No effect is seen from the galactic anticenter, although Clark et al. (1968) see as large a signal from there as from Cygnus. This may be due to the difference in angular resolution of the two detectors or to the poor statistics.

Ögelman (1969) has attempted to explain the mechanism for the OSO-3 γ-ray flux as a series of point sources distributed along the galactic plane in a manner similar to the x-ray sources. According to his calculations an average flux of $5 \cdot 10^{-5}$ γ's $cm^{-2} sec^{-1}$ per source would be required. Our data does not support such a model, since we see no sources above our threshold of $1 \cdot 10^{-5}$ γ' - $cm^{-2} sec^{-1}$ either on or off the galactic plane. If the OSO-3 flux is high by a factor of three however, Ögelman's model becomes more tenable.

ACKNOWLEDGEMENTS

The authors would like to thank J. L. Maynard, A. A. Hruschka, W. Morgan, J. A. Staib, P. Sherry, Dr. A. D. Zych and Dr. W. A. Oran for their assistance in various stages of constructing the equipment and making the flights. Special thanks go to Mesdames P. Balciunas, R. Cassen, C. Conoboy, H. Gelman, M. Paden, M. Samuels, L. Satz and Y. Strauss for their painstaking scanning of the 200,000 pictures. We wish to commend Mr. F. McCreary and the NCAR team for the Palestine flights and Mr. R. Keuser, the Raven crew, and the U.S. Air Force for the flight in Panama.

REFERENCES

Anand, K.C., Daniel, R.R., and Stephens, S.A. 1968, Can. J. Phys., 46, S 484.

Apparao, M.V.K., Proc. Ind. Acad. Sci., 65 A, 349.

Bradt, H., Mayer, W., Naranan, S., Rappaport, S., and Spada, G. 1967, Ap. J. 150, L 199.

Burbidge, G.R. 1958, Ap. J. 127, 48.

Bryam, E.T., Chubb, T.A., and Friedman, H. 1966, Science, 152, 66.

Camerini, U., Davies, J.H., Fowler, P.H., Franzinetti, C., Muirhead, H., Lock, W.O., Perkins, D.H., and Yekutieli, G. 1951, Phil. Mag. 42, 1241.

Charman, W.N., Jelley, J.V., Orman, P.R., Drever, R.W.P., and McBreen, B. 1968, Nature, 220, 565.

Chudakov, A.E., Dadykin, V.L., Zatsepin, V.I, and Nesterova, N.M. 1962, J. Phys. Soc. Japan, 17, Suppl. A-111, 106.

Clark, G.W., Garmire, G., and Kraushaar, W.L. 1968, Ap. J., 153, L 203.

Daniel, R.R., and Sreenivasan, N. 1965, Nuovo Cimento, 35, 391.

Delvaille, J.P., Albats, P., Greisen, K.I., and Ögelman 1968, Can. J. Phys., 46, S 425.

Dolan, J.F., and Fazio G.G. 1965, Rev. Geophys., 3, 319.

Duthie, J.G., Cobb, R., and Stewart, J. 1966, Phys. Rev. Letters, 17, 263.

Duthie, J.G. 1968, Can. J. Phys., 46, S 401.

Elliot, H. 1964, Planetary & Space Science, 12, 657.

Fazio, G.G. 1967, Ann. Revs. Astronomy & Astrophysics, 5, 481.

Fazio, G.G., Helmken, H.F., Cavrak, S.J., and Hearn, D.R. 1968, Can. J. Phys., 46, S 427.

Fazio, G.G., Helmken, H.F., Rieke, G.H., and Weekes, T.C. 1968a, Can. J. Phys., 46, S 451.

_____. 1968b, Ap. J., 154, L 83.

_____. 1968c, Nature, 220, 892.

Fegan, D.J., McBreen, B., O'Mongain, E.P., Porter, N.A., and Slevin, P.J. 1968, Can. J. Phys., 46, S 433.

Felten, J.E. 1968, Ap. J., 151, 861.

Fichtel, C.E., Cline, T.L., Ehrmann, D.A., Kniffen, D.A., and Ross, R.W. 1968, Can. J. Phys., 46, S 419.

Frye, G.M., Reines, F., and Armstrong, A.H. 1966, Jour. Geophys. Res., 71, 3119.

Frye, G.M., and Smith, L.H. 1966, Phys. Rev. Letters, 17, 733.

Frye, G.M., Smith, L.H., Hurschka, A.A., Goff, J.R., and Zych, A.D. 1966, Rev. Sci. Instr., 37, 1340.

Frye, G.M., and Wang, C.P. 1968, Can. J. Phys., 46, S 448.

Garmire, G., and Kraushaar, W.L. 1965, Space Science Revs., 4, 123.

Ginzburg, V.L., and Syrovat-Skii, S.I. 1963, Proc. First Texas Symp. on Relativistic Astrophysics, Univ. of Chicago Press, Chicago, Ill., p. 269.

_____. 1965, Sov. Phys. Uspekhi, 7, 696.

Gould, R.J. 1965, Phys. Rev. Letters, 15, 577.

Gould, R.J., and Burbidge, G.R. 1967, Handbuch der Physik, Vol. 4612 (Berlin Springer-Verlag) pp. 265-309.

Hayakawa, S., Okuda, H., Tanaka, Y., and Yamamoto, Y. 1964, Progress of Theoretical Physics Supplement, 30, 153.

Haymes, R.C., Ellis, D.V., Fishman, G.J., Kurfess, J.D., and Tucker, W.H. 1968, Ap. J., 151, L 131.

Hearn, D.R. 1968, Bull. Am. Phys. Soc., 13, 1435, Preprint, Smithsonian Astrophysical Observatory, Cambridge, Mass.

Morrison, P. 1958, Nuovo Cimento, 7, 858.

Ögelman, H.B., Delvaille, J.P., Greisen, K. 1966, Phys. Rev. Letters, 16, 491.

Ögelman, H. 1969, Nature, 221, 754.

Olsen, H. 1963, Phys. Rev., 131, 406.

O'Mongain, E.P., Porter, N.A., White, J., Fegan, D.J., Jennings, D.M., and Lawless, B. 1968, Nature, 219, 1348.

Oran, W.A., Frye, G.M., and Wang, C.P. 1969, Jour. Geo. Phys. Res., 74, 53.

Poveda, A., and Woltjer, L. 1968, Astro. J., 73, 65.

Quenby, J.J., and Wenk, G.J. 1962, Phil. Mag., 7, 1457.

Savedoff, M.P. 1959, Nuovo Cimento, 13, 12.

Shklovskii, I.S. 1967, Soviet Astron. A. J., 11, 45.

Svennson, G. 1958, Arkiv Fysik, 13, 347.

CAPTIONS FOR FIGURES

Fig. 1 The Spark Chamber and Counter Triggering System

Fig. 2 Effective Spark Chamber Plate Area as a Function of θ, the Angle of Incidence of the Photon K is the Separation Between Counters #2 and #3 in Fig. 1

Fig. 3 Least Squares Fit to Counting Rate as a Function of Residual Atmospheric Depth, (a) Pairs, Texas, (b) Single, Non-Scattering Tracks, Texas, (c) Pairs, Panama

Fig. 4 No. of Events/secθ vs. θ for (a) Pairs and (b) Non-Scattering Single Tracks

Fig. 5 No. of Events vs. Position on Equal Solid Angle Plot
The varying sized bins have equal exposure (sec. 4 c).
The first number in each rectangle is the number of pairs $E_\gamma > 100$ MeV, the second $E_\gamma < 100$ MeV, and the third the number of non-scattering single tracks.

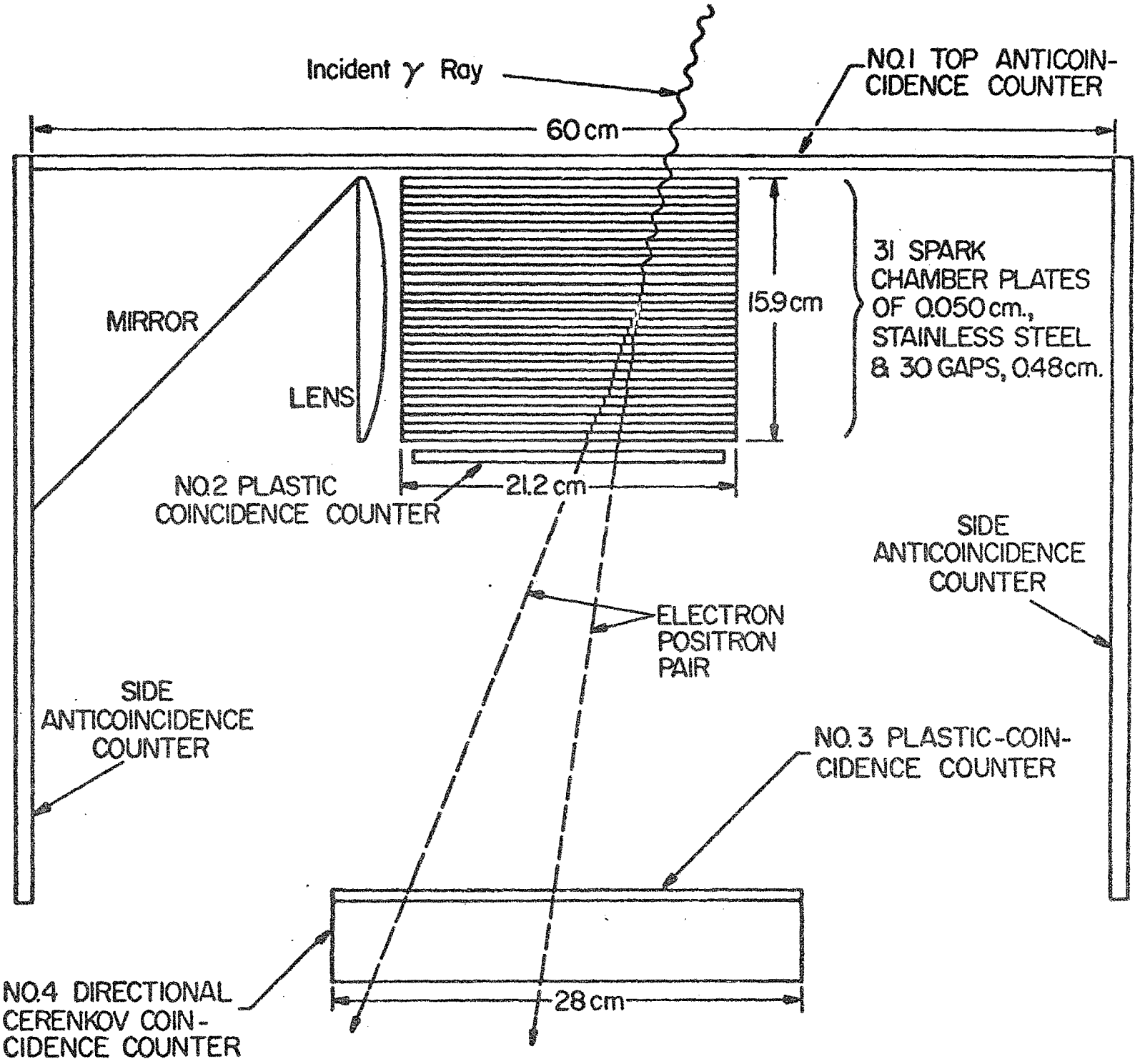
Incident γ Ray
NO.1 TOP ANTICOIN-
CIDENCE COUNTER
60 cm
MIRROR
LENS
15.9 cm
31 SPARK
CHAMBER PLATES
OF 0.050 cm.,
STAINLESS STEEL
& 30 GAPS, 0.48 cm.
NO.2 PLASTIC
COINCIDENCE COUNTER
21.2 cm
SIDE
ANTICOINCIDENCE
COUNTER
ELECTRON
POSITRON
PAIR
SIDE
ANTICOINCIDENCE
COUNTER
NO.3 PLASTIC-COIN-
CIDENCE COUNTER
NO.4 DIRECTIONAL
CERENKOV COIN-
CIDENCE COUNTER
28 cm

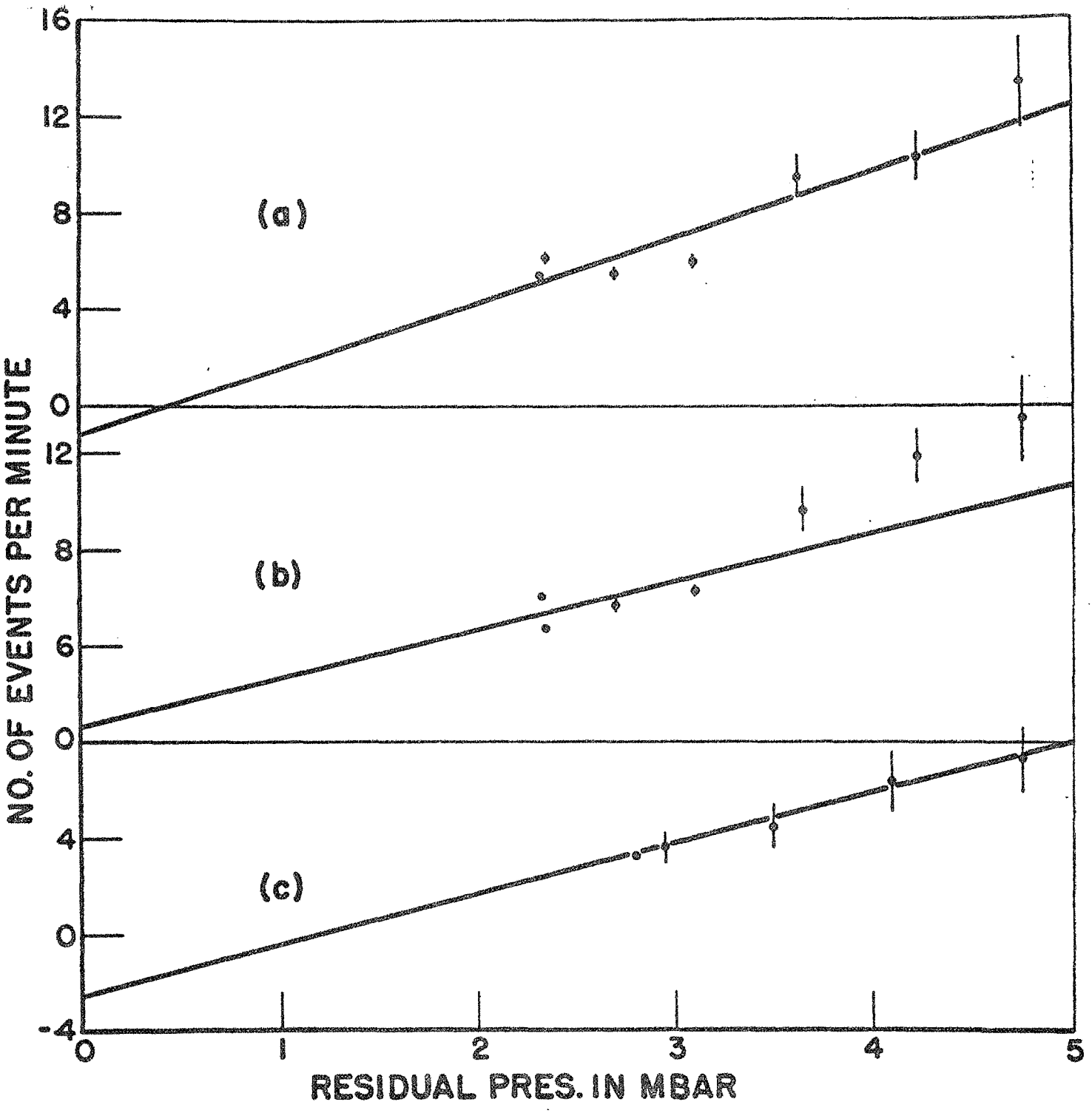
16
12
8
4
0
(a)
12
8
6
0
(b)
4
0
(c)
-4
0
1
2
3
4
5
NO. OF EVENTS PER MINUTE
RESIDUAL PRES. IN MBAR

ARBITARY UNITS
3.0
4.0
5.0
3.0
4.0
5.0
1.0
.99
.98
.97
.96
.95
.94
.93
.92
.91
.90
.89
Cos θ
(b)
(a)

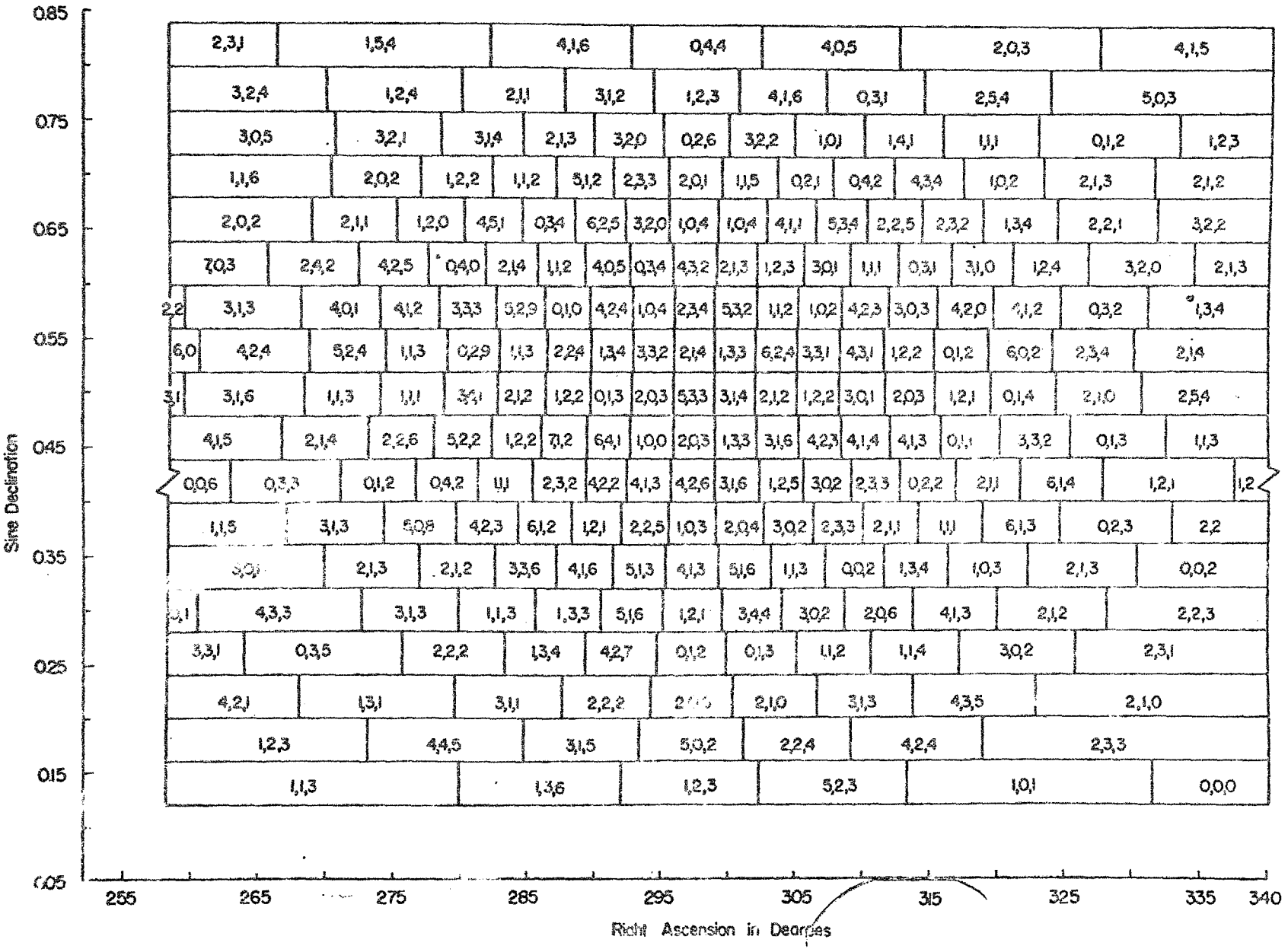
Sine Declination
0.85
0.75
0.65
0.55
0.45
0.35
0.25
0.15
0.05
255
265
275
285
295
305
315
325
335
340
Right Ascension in Degrees

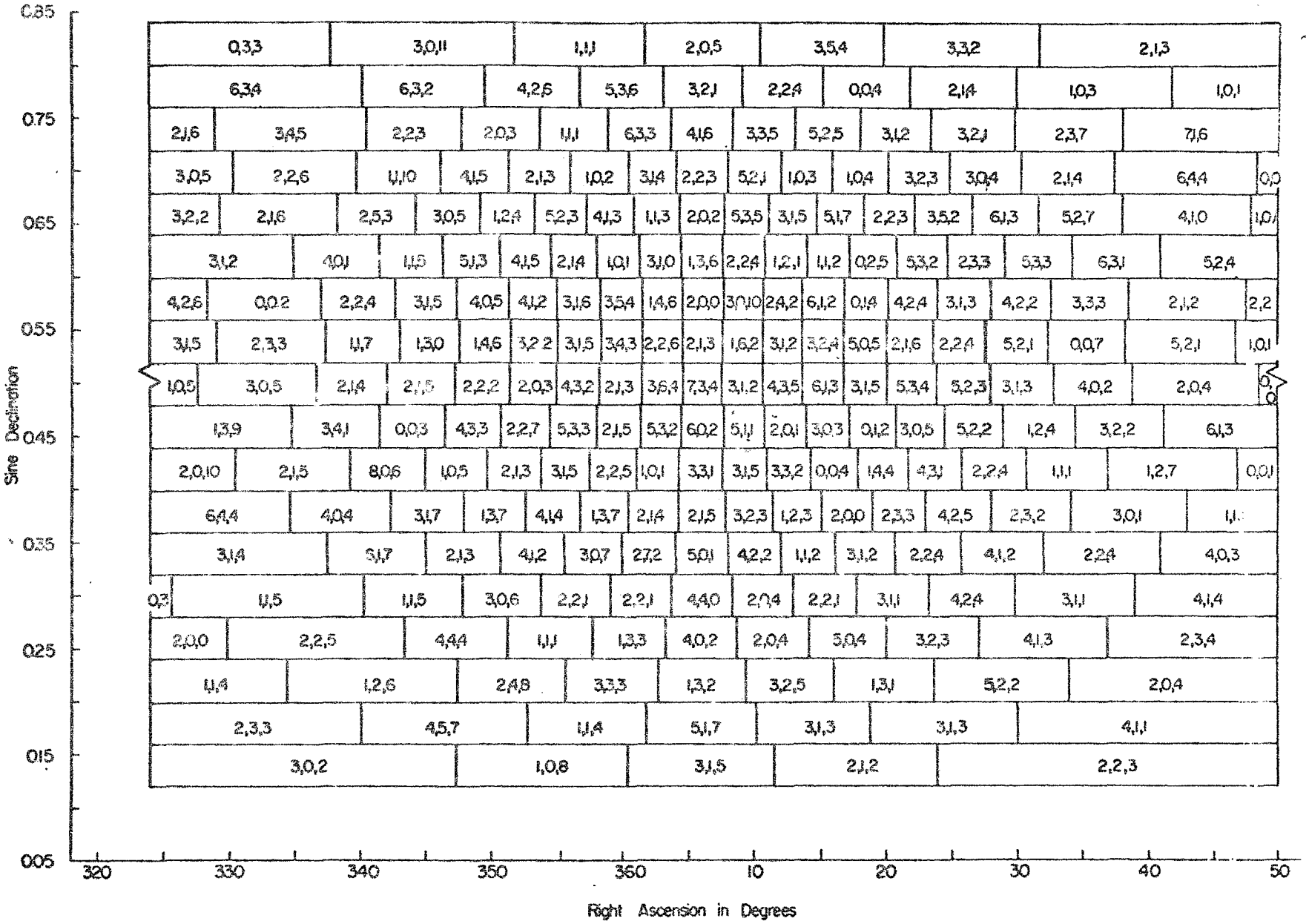
0.85
0.75
0.65
0.55
0.45
0.35
0.25
0.15
0.05
Sine Declination
320
330
340
350
360
10
20
30
40
50
Right Ascension in Degrees

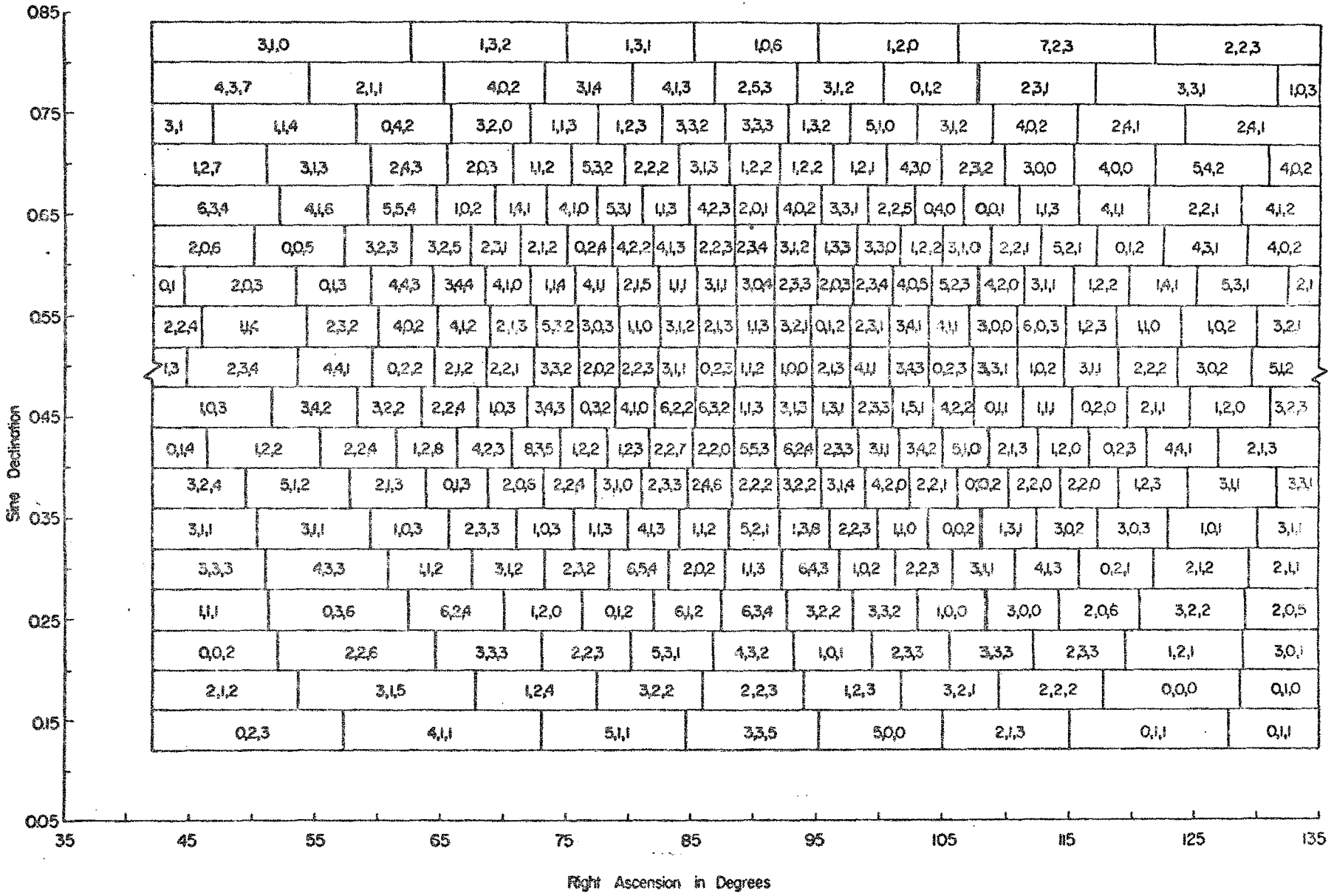
Sine Declination
085
075
065
055
045
035
025
015
005
35
45
55
65
75
85
95
105
115
125
135
Right Ascension in Degrees

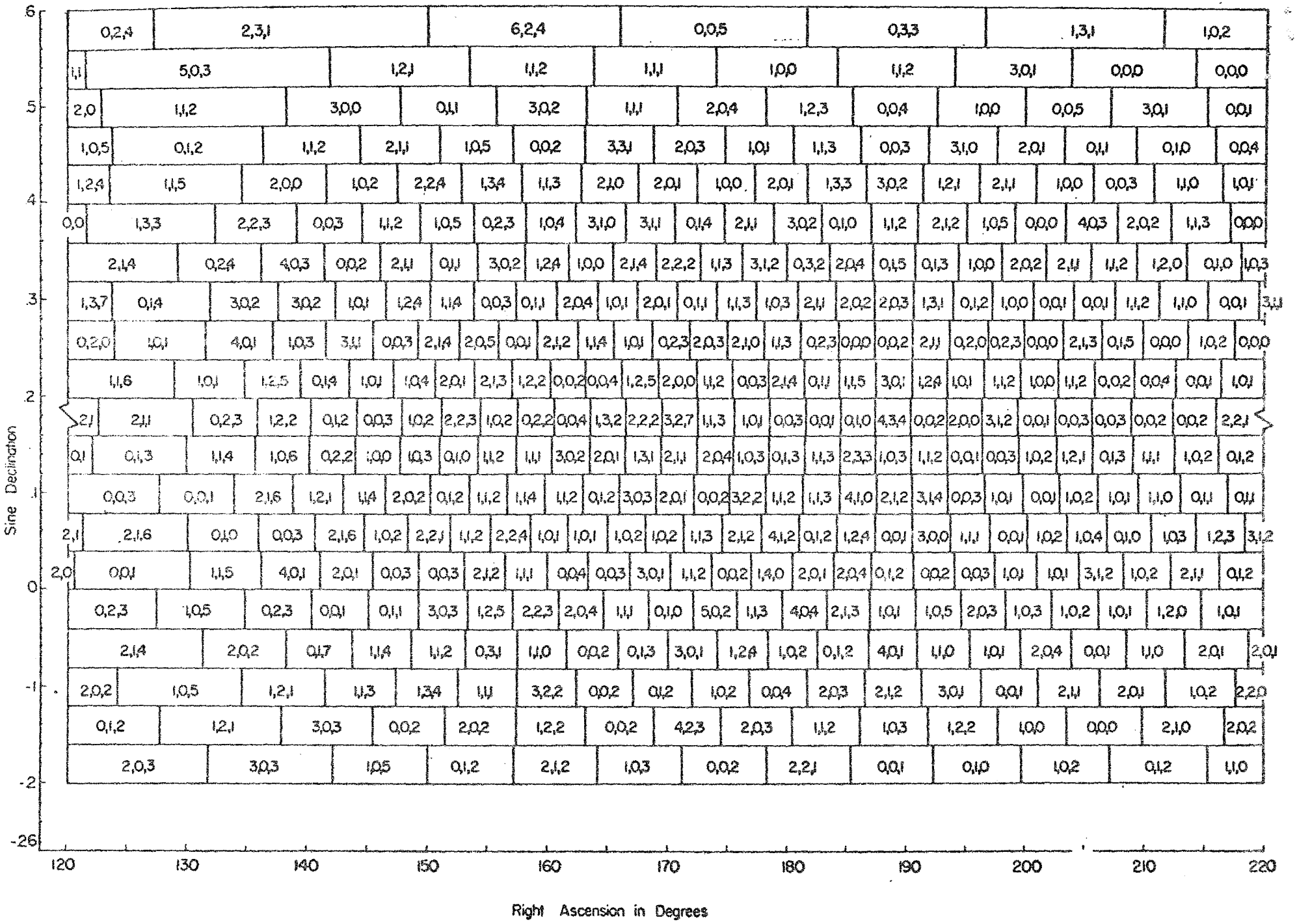
Sine Declination
6
5
4
3
2
1
0
-1
-2
-26
120
130
140
150
160
170
180
190
200
210
220
Right Ascension in Degrees

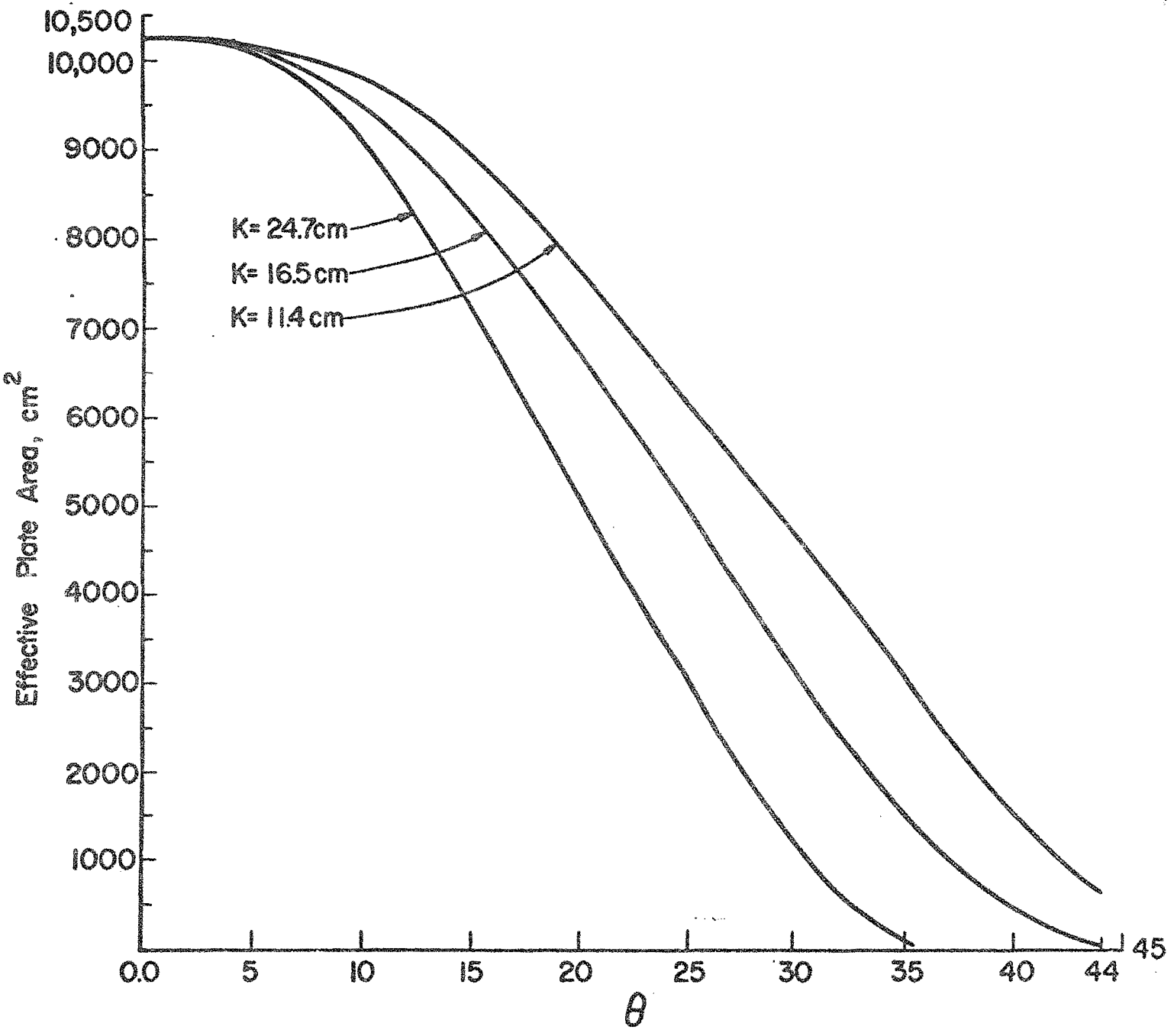
10,500
10,000
9000
8000
7000
6000
5000
4000
3000
2000
1000
Effective Plate Area, cm²
K= 24.7cm
K= 16.5cm
K= 11.4cm
0.0
5
10
15
20
25
30
35
40
44
45
θ